Analysis of Tile-Reinforced Composite Armor
Part 1: Advanced Modeling and Strength Analyses

C. G. Dávila, Tzi-Kang Chen, and D. J. Baker
Army Research Laboratory, Vehicle Technology Center
NASA Langley Research Center, Hampton, VA 23681

Abstract

The results of an analytical and experimental study of the structural response and strength of tile-reinforced components of the Composite Armored Vehicle are presented. The analyses are based on specialized finite element techniques that properly account for the effects of the interaction between the armor tiles, the surrounding elastomers, and the glass-epoxy sublaminates. To validate the analytical predictions, tests were conducted with panels subjected to three-point bending loads. The sequence of progressive failure events for the laminates is described. This paper describes the results of Part 1 of a study of the response and strength of tile-reinforced composite armor.

1. Introduction

The Composite Armored Vehicle (CAV), shown in figure 1, is an Advanced Technology Demonstrator designed and manufactured by United Defense, L.P. (UDLP), of San Jose, CA. The vehicle was designed to demonstrate a reduction of 33% of the combined weight of the armor and the structure compared to the weight of an all-metallic baseline vehicle with equivalent protection. The upper hull of the vehicle consists of a laminate of ceramic tiles sandwiched between a thick glass-epoxy inner hull and a thinner outer hull, as shown in figure 2. To isolate the tiles from the inner hull and to improve damage tolerance, a rubber layer is built into the laminate. Also, the ceramic tiles are bonded to each other and to the surrounding materials with a tough and highly compliant epoxy adhesive that limits the damage propagation to the surrounding tiles.

The proper balance between structural and ballistic performances was optimized in the CAV design by tailoring the interaction between rubber, ceramic tile, glass-epoxy, and adhesive to achieve a design that integrates structure, armor, and signature management. The structural analysis of this anisotropic construction, however, poses several challenges. It was found that, when applied to this type of construction, standard finite element techniques either require extremely high computational resources, or yield unacceptably inaccurate results (Dávila et al., 1996a).

The objective of this paper is to summarize the analysis techniques that were developed to predict the response and strength of CAV components, and to present new test results conducted to study the progressive failure of CAV laminates. The results of Part 2 of the study are presented in Chen et al., 1998, which describes the rate-dependent analysis methods that were developed to characterize the experimentally observed viscoelastic response of the laminates.

2. Finite Element Analysis

Most finite element analyses of thick composite structures rely on so-called thick-shell elements. These computationally efficient elements are based on the Mindlin-Reissner (MR) kinematic assumptions that require that the normal to the shell remains straight and does not elongate. Unfortunately, the unusual through-the-thickness strain distributions in laminates with embedded tiles cannot be represented by conventional shell elements. The complex three-dimensional stress fields in CAV components could be computed by the use of solid elements, but these elements are computationally too expensive to be practical for the analysis of anything other than the smallest components. To mitigate the limitations of solid and shell elements, the following three specialized finite element modeling techniques were developed. These techniques properly account for the effects of tile periodicity and transverse shear flexibility in the rubber mat, and provide the computational efficiency necessary to analyze large hull components.

Figure 1. Composite Armored Vehicle Advanced Technology Demonstrator.

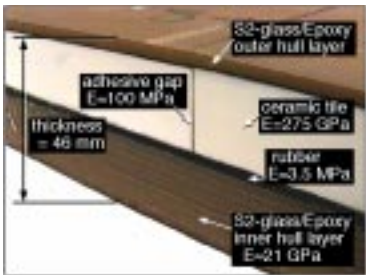

Figure 2. Cross section of CAV upper hull. Approximate values of Young's moduli illustrate the large variations in properties for adjacent materials.

2.1 Element Layering

The strain distribution in tile-reinforced components is significantly different from what might be expected in an isotropic structure. In particular, the compliance of the rubber mat allows some relative motion to occur between the inner and outer portions of the laminate. This relative motion invalidates the Mindlin-Reissner assumptions used for conventional shell finite elements. To ensure the proper transverse shear deformations, a technique called *element-layering* was developed (Dávila et al., 1996a). Element-layering simply consists of modeling the laminated composite shell with more than one thick-shell element through the thickness, each element layer comprising a sublaminate of similar components. The layers are tied together in the model with multi-point constraint (MPC) equations that enforce displacement compatibility at the layer interfaces. The CAV upper hull laminate is modeled with four element layers: 1) a glass-epoxy inner-hull layer; 2) a rubber layer; 3) a layer of tiles and adhesive gaps; and 4) an outer glass-epoxy layer. The structural stiffness obtained from element-layered models agrees very well with the stiffnesses from three-dimensional models. Element-layering is not just applicable to simple flat models. The method was automated with a program that transforms any conventional shell model into multi-layered models. This program reads the information defining the nodes, element connectivities and section properties of a shell model, and writes the new node locations, element layers, section properties and MPC equations.

2.2 Homogenization of Tile Layer

In addition to shear deformation of the rubber layer, it is also essential to include the deformation of the adhesive gaps that bond the tiles to each other. The tiles are placed in patterns consisting of staggered rows. The bondlines between tiles are orders of magnitude smaller than the length of a tile, yet their low stiffness causes more deformation to occur in the adhesive gaps than in the tile when the structure is subjected to applied loads. Unfortunately, it is not normally possible in a full-vehicle analysis to model each discrete tile and its surrounding adhesive interfaces. Therefore, a technique was developed to compute accurately the homogenized material properties of tiles and adhesive (Dávila et al., 1996b). This technique is particularly useful in large-component nonlinear analyses.

2.3 Superelement Models

Superelements can significantly improve the computational efficiency of linear analyses of tile-reinforced structures such as the upper hull of the CAV. The method consists of performing a static condensation of the stiffness matrix for one repeating unit of the structure. Reusing this condensed stiffness can simplify the task of modeling, virtually eliminate the time required to assemble the stiffness matrices, and significantly reduce the problem's solution time. After they are formed, superelements are used much the same way as any other standard element. The user simply specifies the connectivity of the element, its position, and its orientation. Superelements are fully reusable between analyses and allow sharing of data.

The superelements used for this study are based on three-dimensional elements and element-layered technology (Dávila, 1998). The superelements typically encompass one quarter of a tile as well as one half of the adhesive gap on two faces of the tile, as shown in figure 3. Half-tile and full-tile superelements were also created by combining two and four quarter-tile superelements, respectively. For each superelement, all degrees of freedom except those of the nodes along the four vertical faces are eliminated through static condensation. The finite element code ABAQUS (Anon., 1996) was found to be particularly well suited for the superelement analysis of CAV components. The bundled post-processor ABAQUS/POST supports all ABAQUS superelement options and provides a convenient method for displaying superelement results. The example shown in figure 4 illustrates strain and displacement results within selected superelements in a symmetric model of a plate subjected to three-point bending loads.

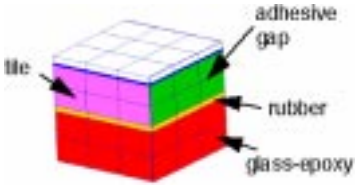

Figure 3. Superelement of a quarter of a tile. All nodes except those on the four vertical faces are eliminated by static condensation.

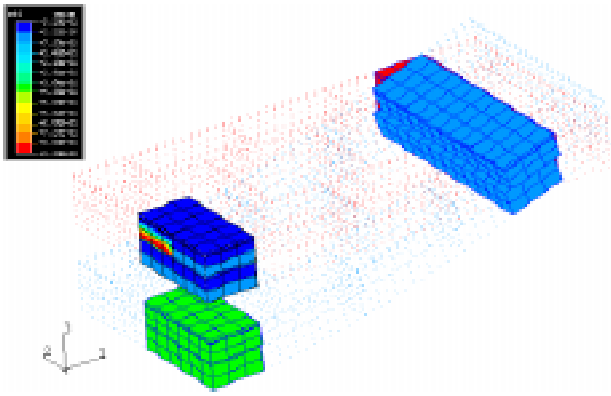

Figure 4. Superelement model of a plate subjected to a three-point bending load. Strain and deformation results are shown inside selected superelements (ABAQUS/POST).

3. Experimental Results

A large number of CAV components have been extensively tested by UDLP, and all have been shown to withstand automotive, gunfiring and specified collision loads. In addition to these tests, the Vehicle Technology Center (VTC) conducted material characterization and structural tests to examine in detail the progressive failure of CAV panels subjected to bending (Dávila et al., 1997). Three 85-cm-long panels manufactured by UDLP were tested by VTC. Specimens Number 1 and Number 3 are 39.4 cm wide, and Specimen Number 2 is 31.12 cm wide.

The experimental procedure is composed of two parts. The first part consists of a series of low-load tests that were conducted to characterize the viscoelastic response of the plates. For Specimen Number 2, these tests are labeled S2-1 through S2-11 herein. The second part of the procedure is the destructive evaluation of the three specimens. After completion of the tests, it was observed that the plates had accumulated some damage during the low-load tests, before the initiation of the destructive test.

3.1 Stiffness and Strength Degradation

One particularly interesting test result that was not identified by UDLP is that the response of CAV panels is strongly viscoelastic, as can be observed from the hysteresis loops in the load-deflection curves shown in figure 5. The analysis of the viscoelastic response is the topic of a second paper, (Chen et al., 1998).

The test results also indicate that the stiffness and strength of the panels degrade with the repeated application of relatively low loads. In general, the low-load damage events were too small to be noticed without a direct comparison between consecutive tests. For example, the first damage event occurred during the second test, S2-2. The load-displacement plot shown in figure 5 is an overlay of the two consecutive tests S2-2 and S2-3. At a load of 6,160 N, a failure event caused a sudden 37% reduction in the stiffness of the panel. This load is only 5% of the ultimate failure load for this panel. By the time of test S2-3, however, some of the stiffness had been regained through viscoelastic relaxation. Evidence of a failure event is also apparent in the strain gage results shown in figure 6. This damage event that occurred during test S2-2 and other subsequent damage events went unnoticed until after the test program had been completed. The damage zones may consist of regions of fiber buckling caused by the inplane compressive loads associated with bending.

The effect of repeated loads on Specimen Number 2 was examined by representing the history of the response characteristics of this specimen on a single chart, which is shown in figure 7. For each of the 12 tests, the stiffness was linearized by one, two or three tangents, as required for a good fit of the results of the first load increment of the tests (the first load increment is from zero load until the load rate is reversed). For example, two dashed lines drawn in figure 5 represent the first two tangents for test S2-2, which are shown in figure 7 as points 1 and 2. The first data point represents the initial stiffness in units of N/cm. Tests S2-6 through S2-9 were conducted with the outer hull surface subjected to tension. In all other tests, the outer hull surface was subjected to compression. This comparison is not strictly rigorous, since the tests were performed at different load rates, and the tangent stiffnesses are not computed at the same loads. The results show that the tests configured with the outer surface subjected to tension are approximately 18% stiffer than the tests with the opposite configuration. In all cases with the outer hull placed in compression, the tangent stiffness decreased with increased load. The initial

stiffness of the panel decreased significantly during test S2-2, and continued to decrease during subsequent tests that placed the outer hull in compression. The line connecting all initial stiffnesses of the specimens with the outer hull in compression is referred to as the stiffness degradation line in figure 7. The stiffness degradation line decreases monotonically, except for a minor increase with test S2-11.

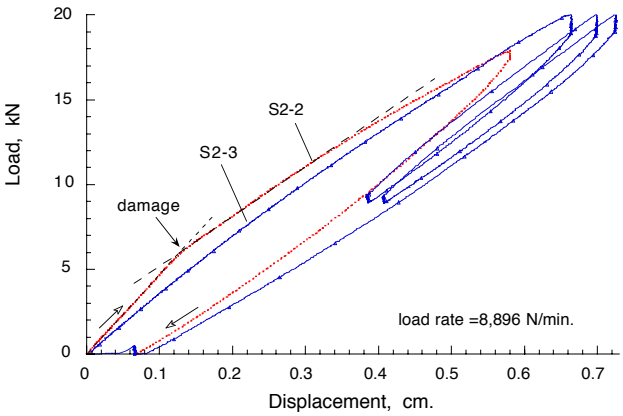

Figure 5. Load-displacement curves for tests S2-2 and S2-3. The knee at 6,160 N for S2-2 is not present in S2-3.

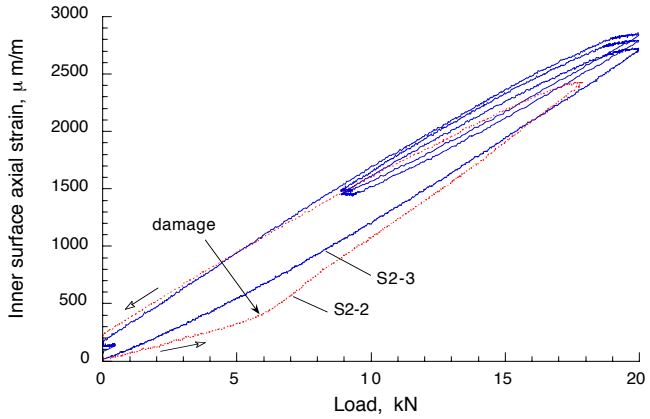

Figure 6. Inner hull surface strains for tests S2-2 and S2-3 at gage location BL (location shown in figure 8).

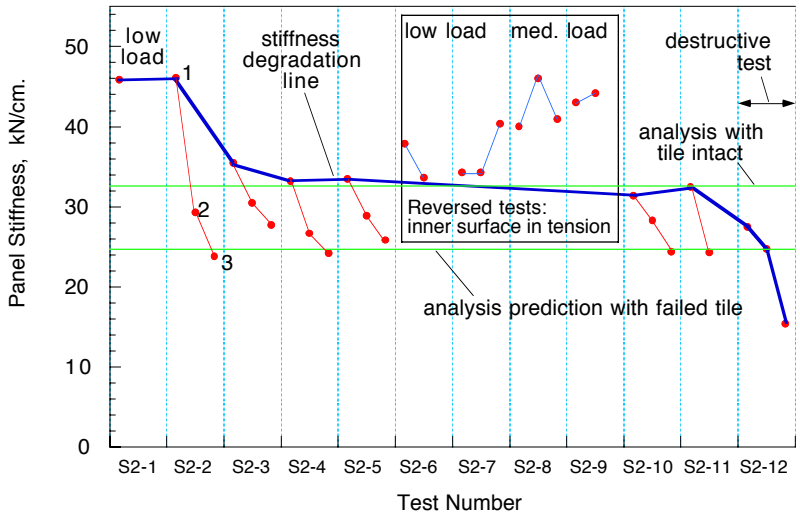

Figure 7. History of response for Specimen Number 2. The stiffness degradation line indicates that the panel exhibits a progressive stiffness and strength degradation with the application of repeated loads.

3.2 Failure Progression

The three panels were tested to failure by subjecting them to three-point bending loads. Specimen Number 1 was tested with the outer hull surface facing down so that it was loaded in tension. Specimens Number 2 and 3 were tested to failure with the outer hull surface loaded in compression, as shown in the photographs in figure 8. The tests were recorded on video tape, and the sequence of failure events was later correlated to the load-displacement curves, also shown in figure 8. After the tests, the outer hull layers were peeled off, and the damage to the tiles and adhesive bondlines was inspected.

The load-displacement curves in figure 8 clearly indicate that the characteristics of the failure progression can vary significantly, even among panels with similar configurations. It is also apparent that these panels can support loads far exceeding the loads associated with the initial failure events. Table 1 summarizes the sequence of failure events leading to the destruction of each specimen.

Table 1. Comparison of failure progression for three plates subjected to three-point bending loads.

	Specimen 1	Specimen 2	Specimen 2
Characteristics	base configuration; outer surface in tension.	narrower than base configuration and outer surface in compression.	transverse tile pattern; outer surface in compression.
Failure 1	failure of adhesive bond.	tile failure preceded and followed by adhesive bond failures and localized damage in outer hull.	tile and adhesive failures.
Failure 2	tile breaks.	delamination of outer hull.	delamination of outer hull.
Failure 3	delamination of outer hull.	debond at tile/rubber interface.	debond at tile/rubber interface.
Failure 4	bridging of crack across specimen; large drop in stiffness.	tensile failure of phenolic layer (inner hull).	N/A
Failure 5	debonding of phenolic layer.	complete debond of rubber layer.	N/A

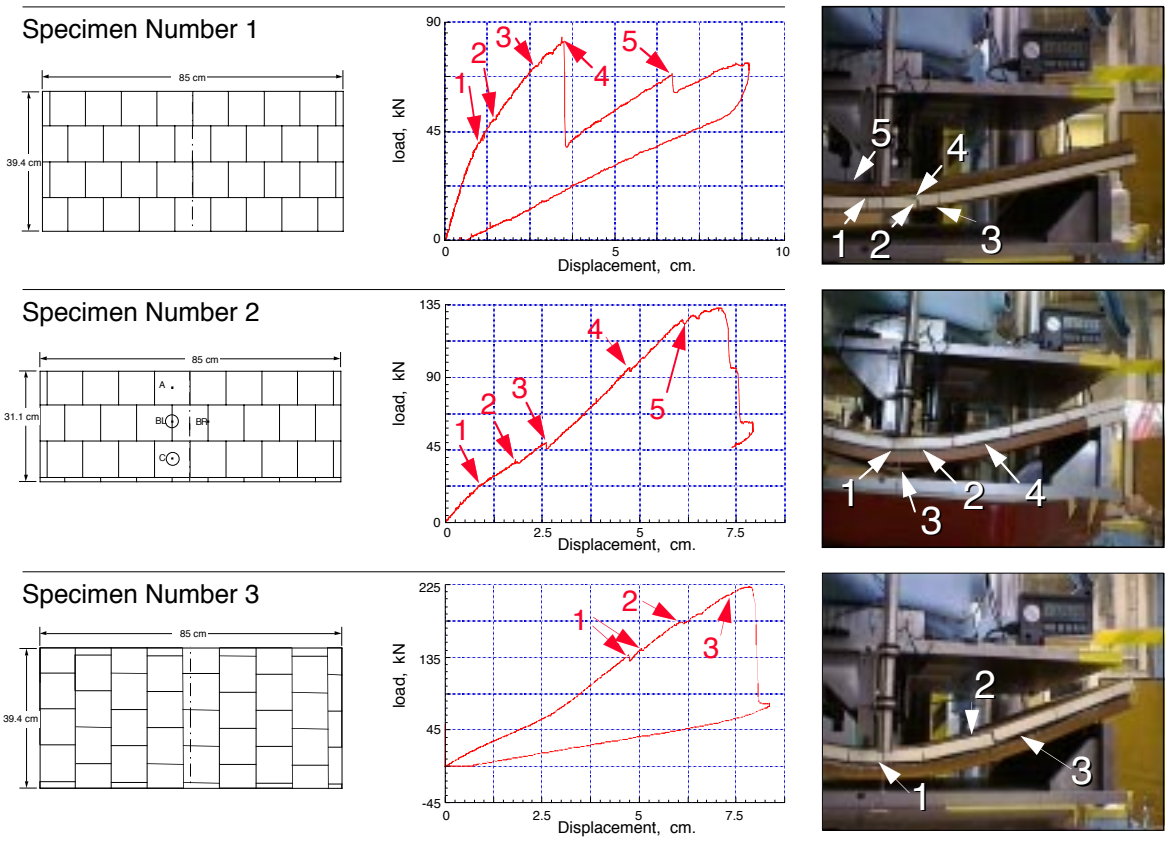

Figure 8. Progressive failure events for three CAV panels subjected to three-point bending loads.

Table 2 provides a summary of the strength of the three specimens. The apparent failure initiation load per unit width is associated with the first failure event that noticeably released strain energy as indicated by the sharp discontinuities in the load-deflection plots of figure 8. However, after a detailed analysis, other failures associated with low-intensity loads were identified that were not noticed during the tests.

Table 2. Comparison of strength characteristics for three panels subjected to three-point bending loads.

Specimen number	Apparent initial failure load/width (N/cm)	Maximum load/width (N/cm)	Deflection at maximum load (cm)
1	902	2,031	3.56
2	1,144	4,150	7.11
3	3,389	5,534	7.87

As a result of the compliant elastomers in the laminate, many failure events did not emit audible sounds or cause noticeable energy releases. Consequently, these failure events were not identified during the tests, but were revealed after comparison to previous test results.

The test results also show large differences in response and strength between panels, even among panels possessing similar configurations. For example, the stiffness of a panel is higher for the loading condition that places the outer hull in tension rather than in compression. All panels were capable of sustaining loads several times greater than their failure initiation loads. However, the repeated application of loads as small as 5% of the ultimate load causes an accumulation of damage in the specimen and a progressive degradation of the stiffness and strength of the specimen**.**

Analysis played a key role in the interpretation of the results. The tile failure loads and the responses after failure initiation were calculated, and the predicted results correlated well with experimental results when three-dimensional superelement models were used, and tensile fracture of the tile was assumed. The predicted panel stiffnesses before and after tile fracture for Specimen Number 2 are shown by the two horizontal lines in figure 7. The failure of the tile, however, is less pronounced than expected, since the tile appears to have failed by crumbling, rather than by snapping. This mode of failure may be the result of the tight confinement of the tile within the laminate and the fact that tile fracture is not the first failure event. It was observed that tile fracture is preceded by other damage events that appear to be associated with yielding of the adhesive and fiber crippling in the outer hull.

Concluding Remarks

An analytical and experimental study was conducted to gain a better understanding of the response and strength of upper hull components of the Composite Armored Vehicle. Three panels were tested to destruction. The sequence of failure events was studied by comparing the loads, displacements, strains, videotaped recordings of the tests, and post-test inspections of the tiles and the adhesive. The test results show large differences in response and strength between panels, even for panels with similar configurations. For example, the stiffness of a panel is higher for a loading condition that places the outer hull in tension rather than in compression. Also, the stiffness of the plates with tiles placed in longitudinal rows is higher than for tiles placed in transverse rows. All panels were capable of sustaining loads several times greater than their failure initiation loads. However, the repeated application of loads as small as 5% of the ultimate load causes an accumulation of damage in the specimen and a progressive degradation of the stiffness and strength. Because of the compliant elastomers in the laminate, many failure events did not emit audible sounds or cause noticeable energy releases. Consequently, these failure events were not identified during the tests, but were revealed after comparison of results with results of previous tests.

Analysis played a key role in the interpretation of the experimental results. The prediction of the failure load was based on tensile fracture of the tile. However, the tests also indicated that the fracture of a tile is not the first failure event, and that it is preceded by other localized damage events such as yielding of the adhesive and fiber crippling in the outer hull.

References

1. Anon., *ABAQUS Standard User's Manual, V 5.6*, Hibbitt, Karlsson & Sorensen, Inc., Pawtucket, RI, 1996.
2. Chen, T.K., Dávila, C.G. and Baker, D.J., *Analysis of Tile-Reinforced Composite Armor, Part 2: Viscoelastic Response*, 21st Army Science Conference, Norfolk, VA, June 1998.
3. Dávila, C.G., Smith, C. and Lumban-Tobing, F., *Analysis of Thick Sandwich Shells with Embedded Ceramic Tiles*, Proceedings of the 11th DoD/NASA/FAA Conference on Fibrous Composites in Structural Design, Fort Worth, TX, August 1996.
4. Dávila, C.G. and Chen, T.K., *CAV Tile Layer Homogenization and Parametric Study*, VSD NR 96-03, U.S. Army VTC, NASA Langley Research Center, Hampton, VA, July 1996.
5. Dávila, C.G., Chen, T.K. and Baker, D.J., *Viscoelastic Response and Strength of Tile-Reinforced Composite Armor*, VTC NR-97-05, U.S. Army VTC, NASA Langley Research Center, Hampton, VA, October. 1997.
6. Dávila, C.G., *Superelement Analysis of Tile-Reinforced Composite Armor*, Proceedings of the 11th Worldwide ABAQUS User's Conference, Newport, RI, May 1998.